ACS OMEGA

Article

Cite This: ACS Omega 2018, 3, 898−905

Solution Plasma Process-Derived Defect-Induced Heterophase Anatase/Brookite TiO_2 Nanocrystals for Enhanced Gaseous Photocatalytic Performance

Sudhagar Pitchaimuthu,[†,⊥,#] Kaede Honda,[‡] Shoki Suzuki,[‡] Akane Naito,[‡] Norihiro Suzuki,[‡] Ken-ichi Katsumata,[‡] Kazuya Nakata,[†,‡] Naoya Ishida,[†,‡] Naoto Kitamura,[†,‡] Yasushi Idemoto,[†,‡] Takeshi Kondo,[†,‡] Makoto Yuasa,[†,‡] Osamu Takai,[§] Tomonaga Ueno,[∥] Nagahiro Saito,[∥] Akira Fujishima,[†] and Chiaki Terashima*[,†]

[†]Photocatalysis International Research Center, Research Institute for Science & Technology, and [‡]Faculty of Science and Technology, Tokyo University of Science, 2641 Yamazaki, Noda, Chiba 278-8510, Japan

[§]Materials and Surface Engineering Research Institute, Kanto Gakuin University, 1162-2 Ogikubo, Odawara, Kanagawa 250-0042, Japan

[∥]Department of Materials, Physics and Energy Engineering, Graduate School of Engineering, Nagoya University, Furo-cho, Chikusa-ku, Nagoya 464-8603, Japan

[⊥]Multi-functional Photocatalyst and Coatings Group, SPECIFIC, College of Engineering, Swansea University (Bay Campus), Swansea SA1 8EN, Wales, U.K.

S *Supporting Information*

ABSTRACT: We report a simple room-temperature synthesis route for increasing the reactivity of a TiO_2 photocatalyst using a solution plasma process (SPP). Hydrogen radicals generated from the SPP chamber interact with the TiO_2 photocatalyst feedstock, transforming its crystalline phase and introducing oxygen vacancy defects. In this work, we examined a pure anatase TiO_2 as a model feedstock because of its photocatalytic attributes and well-characterized properties. After the SPP treatment, the pure anatase crystalline phase was transformed to an anatase/brookite heterocrystalline phase with oxygen vacancies. Furthermore, the SPP treatment promoted the absorption of both UV and visible light by TiO_2. As a result, TiO_2 treated by the SPP for 3 h showed a high gaseous photocatalytic performance (91.1%) for acetaldehyde degradation to CO_2 compared with the activity of untreated TiO_2 (51%). The SPP-treated TiO_2 was also more active than nitrogen-doped TiO_2 driven by visible light (66%). The overall photocatalytic performance was related to the SPP treatment time. The SPP technique could be used to enhance the activity of readily available feedstocks with a short processing time. These results demonstrate the potential of this method for modifying narrow-band gap metal oxides, metal sulfides, and polymer composite-based catalyst materials. The modifications of these materials are not limited to photocatalysts and could be used in a wide range of energy and environment-based applications.

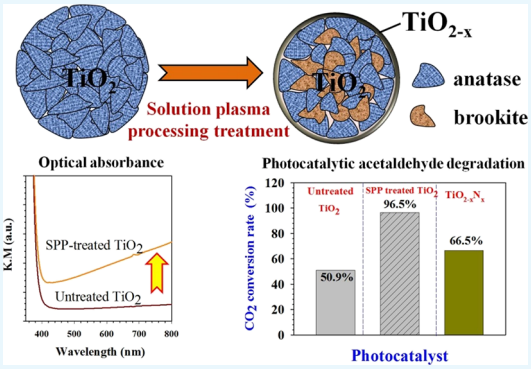

INTRODUCTION

In recent years, TiO_2 has attracted interest owing to its promising photocatalytic functionality, which has a variety of applications, including energy conversion,[1,2] environmental remediation,[3,4] photochemical storage,[5] self-cleaning,[6] biomedical diagnosis[7] and therapy,[8] and photocatalytic wall coating.[9] However, the wide band gap energy of TiO_2 (~3−3.2 eV) limits harvesting of solar energy in the visible wavelength region.[10] Therefore, much research has focused on improving the visible light-harvesting capabilities of TiO_2 for outdoor photocatalytic applications. A recent strategy based on band gap engineering of the TiO_2 lattice through metal and nonmetal doping has been shown to effectively improve the light harvesting of TiO_2.[11−16] However, dopant-induced defects in the TiO_2 lattices often have detrimental effects, introducing charge carrier trapping and recombination sites, which negatively affect the photoactivity.[17] Therefore, promoting the photocatalytic activity of the TiO_2 crystal lattice without producing any adverse effects remains challenging.

Recently, hydrogenated or defect-induced "black TiO_2" (H-TiO_{2-x}) has shown effective photon harvesting at longer wavelengths up to ~800 nm with appreciable photocatalytic

Received: November 1, 2017
Accepted: January 11, 2018
Published: January 24, 2018

DOI: 10.1021/acsomega.7b01698
ACS Omega 2018, 3, 898−905

activity.[18,19] The surface disorder (band edge tail) and oxygen vacancies (V_o) formed by the hydrogen treatment can increase the electronic charge carriers to improve the electronic conductivity and modify the band gap of TiO_2. These effects increase the ability of TiO_2 to absorb visible light. Many techniques have been applied to synthesize H-TiO_{2-x}, including high-pressure thermal treatment techniques, chemical oxidation and reduction methods, high-energy particle bombardment (hydrogen plasma, argon, and electron), and electrochemical techniques.[20−22] Among these techniques, it is believed that hydrogen dopants form Ti−H and O−H bonds with TiO_2. These defects introduce mid-gap states, which change the color of pristine TiO_2 from white to blue, green, or black. Although these methods are capable of synthesizing H-TiO_{2-x}, the requirements of high processing temperatures (~500 °C), vacuum conditions, lengthy process durations, and complex multistep processes limit their practical implementation.

To address these limitations, room-temperature solution plasma process (SPP) techniques might offer a promising alternative to vacuum techniques.[23] SPP is a nonthermal physical tool for synthesizing metal nanoparticles, metal oxide nanoparticles, and polymer-passivated metal oxides.[24−27] In SPP techniques, plasma generated inside a liquid (water) acts as a source for generating highly reactive species, including radicals, atoms, and ions owing to the low dissociation energy of water. The generation of hydroxyl radicals from an SPP can drive oxidation processes at a higher oxidation potential than that possible with other oxidative species. Conversely, hydrogen atoms from oxidative species are highly energetic and can rapidly diffuse into the target TiO_2 material to produce hydrogenated TiO_2. To date, the SPP technique has been applied to in situ synthesis of H-TiO_{2-x} with titanium (Ti) rods for anode and cathode.[28] During plasma generation in the liquid, hot spots are created on the oxidized Ti electrode surface owing to the Joule heating effect, which induces the pair of metallic Ti electrodes to react, producing H-TiO_{2-x}.[28] Using a similar technique, Yonezawa and co-workers[29] synthesized tungsten (W)-doped black TiO_2. The SPP technique has processing advantages for the synthesis of defect-induced TiO_2; however, the output quantity is not high compared with those of vacuum techniques because vacuum techniques use presynthesized TiO_2 powder as a feedstock for synthesizing defect-induced TiO_2. Thus, if SPP-based processing could use presynthesized TiO_2 as a feedstock and high outputs could be achieved, it would become a suitable method for applications on an industrial scale.

In this work, for the first time, we used SPP to produce TiO_{2-x} on a gram scale, from commercially available TiO_2 solid (ST-1 TiO_2, Ishihara Sangyo Kaisha Ltd., Japan) as a feedstock. This ST-1 TiO_2 powder features a pure anatase phase. A schematic illustration of the SPP technique is depicted in Scheme 1. In this setup, plasma emission is generated by a pair of tungsten arc electrodes. The emission center of the plasma is located in a gas phase, surrounded by an aqueous liquid phase. This results in two interfaces, namely, plasma/gas and gas/liquid. Furthermore, an ion sheath forms near the gas/liquid interface, and the resultant plasma is confined by a condensed phase, which produces the unique features of a solution plasma.[28] This solution plasma drives extremely rapid reactions through activated chemical species and radicals (hydrogen, hydroxyl, and oxygen) under a high pressure. Among these active chemical species, the hydrogen radical (H^{+}*) is mainly responsible for modifying feedstock particles dispersed in the

Scheme 1. Schematic Illustration of the SPP Technique (Note That the Nitrogen Gas Is Applied through the Cathode Cavity)

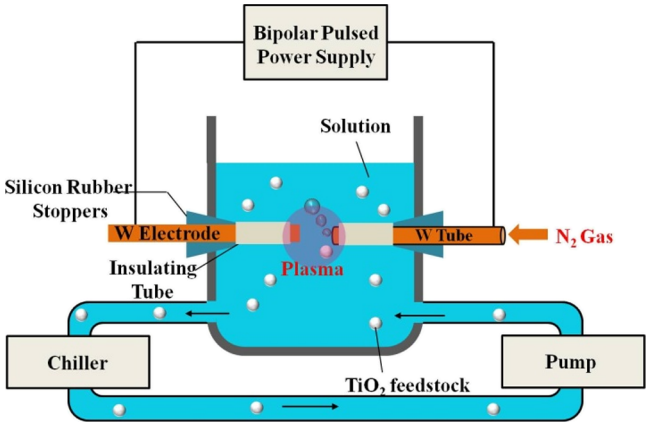

electrolyte. Nitrogen gas is applied to the reaction chamber through the central cavity of the cathode electrode, which energetically produces bubbles in the solution plasma and facilitates the interaction between the feedstock particles and the hydrogen free-radical species. A video of the interaction between the nitrogen bubbles and the plasma was recorded with a high-speed camera (Movie S1, Supporting Information). Further experimental details of the SPP technique and its parameters are given in the Supporting Information.

RESULTS AND DISCUSSION

Structural Analysis. The color of the ST-1 TiO_2 powder turned from milky white to light brown (Figure S1, Supporting Information) after the SPP treatment. This color change indicated the modification of the pure anatase ST-1 TiO_2 by either induction of defects or reduction of TiO_2. However, the X-ray diffraction (XRD) spectra of untreated and SPP-treated ST-1 TiO_2 powder showed no notable changes (Figure S2, Supporting Information). We analyzed the morphology of the SPP-treated ST-1 TiO_2 sample using high-angle annular dark-field (HAADF) imaging in a scanning transmission electron microscope. Figure 1a−k shows the HAADF−scanning transmission electron microscopy (STEM) results of the SPP-treated ST-1 TiO_2. In Figure 1a, lattice fringes at two different places indicated in yellow and red boxes were examined in detail (Figure S3, Supporting Information). The red color indicates a lattice plane distance of 0.19 nm (Figure 1b) with an interplanar angle of 90°, corresponding to the anatase (100) plane. The yellow-highlighted lattice (Figure 1c) shows a plane distance of 0.34 nm, indicating the anatase (101) plane. The crystalline lattice was analyzed at random locations, which consistently showed the presence of (100) and (101) anatase phases. Further investigations of the influence of the SPP treatment on the bulk TiO_2 crystals (Figure 1d,g) showed 0.45 ± 0.025 nm and 0.35 ± 0.025 nm lattice distances (Figure 1e,h). The corresponding fast Fourier transform images in Figure 1f,i confirmed that these lattice patterns derived from brookite (100) and (010) crystalline phases, respectively (Figure S4, Supporting Information). A small discrepancy in the brookite lattice distance value exists because of the different measurements using simulation software and the scale bar in TEM images. The presence of a heterocrystalline phase of anatase/brookite was unexpected from this room-temperature

DOI: 10.1021/acsomega.7b01698
ACS Omega 2018, 3, 898−905

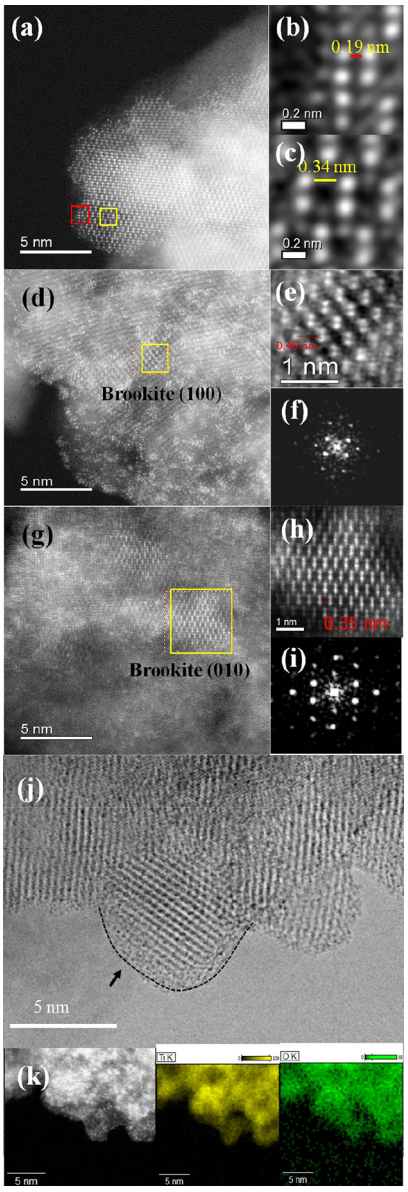

Figure 1. HAADF−STEM image of the SPP-treated TiO_2 powder (a) on a 5 nm scale; high-resolution lattice image on a 0.2 nm scale indicated in (b) the red box (anatase (101) phase) and (c) the yellow box (anatase (001) phase) in (a); HAADF−STEM images of the SPP-treated ST-1 TiO_2 powder measured in the bulk-region (d−f) brookite (100) phase and (g−i) brookite (010) phase. (j) TEM image of the SPP-treated ST-1 TiO_2 (the dotted line represents the amorphous shell); and (k) energy-dispersive X-ray spectroscopy results obtained from (a) (Ti and O).

process; brookite is usually formed at a high temperature (160−500 °C).[30−33]

Saito and co-workers demonstrated that H^+ radicals generated from a similar type of SPP reaction, which played a crucial role in reducing gold precursor salt into gold nanoparticles.[34,35] Analogous to the gold nanoparticle formation by the SPP treatment, it is anticipated that H^+ radical species transform anatase feedstock crystals to a heterocrystalline phase (anatase/brookite). Surprisingly, Figure 1j shows that the SPP treatment created a thin amorphous, disordered shell around the TiO_2 particles with a thickness of approximately 1−2 nm (for the comparison of the STEM images of untreated and SPP-treated ST-1 TiO_2, see Figure S5, Supporting Information). This disordered amorphous layer was likely formed by hydrogen radicals in the SPP. As outlined in Scheme 1, during the water plasma generation, the tungsten electrodes generated positive H^+ ions and negative OH^- and O_2^- ions.[36] Because the ionic masses of the negative species are larger than those of the positive H^+ ions, the heavier species remained in the plasma zone. However, the positive H^+ ions rapidly came into contact with the plasma/liquid interface. In this region, the circulated feedstock, ST-1 TiO_2, interacted with the H^+ species. Bombardment of the TiO_2 surface by H^+ removed the oxygen atoms and created oxygen vacancies (V_o) in the TiO_2. Thus, a thin amorphous defect layer forms on the particle surface. In addition, the energetic H^+ radical species reacted with the TiO_2 lattice and rearranged the atomic alignment. This process induces a mixture of anatase (101) and (001) as well as brookite (100) and (010) crystalline facets.

The chemical composition and chemical binding environment of the untreated and SPP-treated ST-1 TiO_2 were examined by X-ray photoelectron spectroscopy (XPS). Figure 2a shows the Ti 2p core XPS results of pristine and SPP-treated

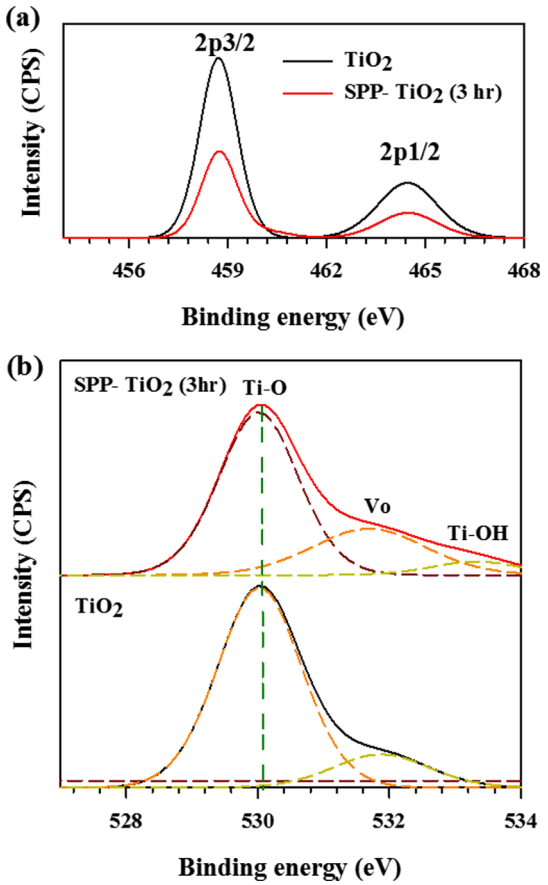

Figure 2. XPS results of the untreated and SPP-treated ST-1 TiO_2: (a) Ti 2p and (b) O 1s core spectra.

TiO_2. Two major peaks were observed at 458.6 and 464.4 eV, corresponding to Ti $2p_{3/2}$ and Ti $2p_{1/2}$, respectively.[37] There was no major change in the Ti 2p position before and after the SPP treatment. Furthermore, no traces of Ti^{3+} could be seen in these spectra. Although we observed an amorphous TiO_{2-x} layer on the SPP-treated particles (Figure 1j), the XPS results showed no Ti^{3+} peak (Figure 2a). Thus, the SPP treatment did

DOI: 10.1021/acsomega.7b01698
ACS Omega 2018, 3, 898−905

not produce Ti^{3+} centers, and the observed amorphous shell layer derived from oxygen vacancies. To confirm the structure, we examined the O 1s spectrum (Figure 2b) of the SPP-treated TiO_2. In Figure 2b, a notable difference in the peak position of the shoulder at ~532.4 eV was observed after the SPP treatment. In general, oxygen atoms in a TiO_2 lattice exhibit three possible chemical states, namely, lattice oxygen O_L at 530.7 eV, surface hydroxyl oxygen at 532.5 eV, and surface-adsorbed oxygen (Ti−OH) at 533.6 eV.[38,39] From Gaussian fitting analysis, the additional peak observed at 533.4 eV indicated the adsorption of hydroxyl groups on the TiO_2 surface. As discussed earlier, the removal of oxygen atoms from the outer surface by H^+ radical species led to the adsorption of hydroxyl groups from the atmosphere.[39] Atmospheric oxygen species are not able to intercalate into a fully oxidized TiO_2 surface.[40] When oxygen vacancies were created on the TiO_2 surface, oxygen adatoms attach to these sites and form hydroxyl groups through $O_2{}^{*-}$ radicals.[40] Therefore, the observed hydroxyl oxygen species peak from the SPP-treated ST-1 sample implies that the SPP treatment created oxygen vacancies on the TiO_2 surface. This result also explains the amorphous layer found in the STEM results (Figure 1j).

Optical Analysis. Analysis of optical absorbance can provide qualitative information on the TiO_2 band gap energy structure before and after the SPP treatment. Figure 3 shows

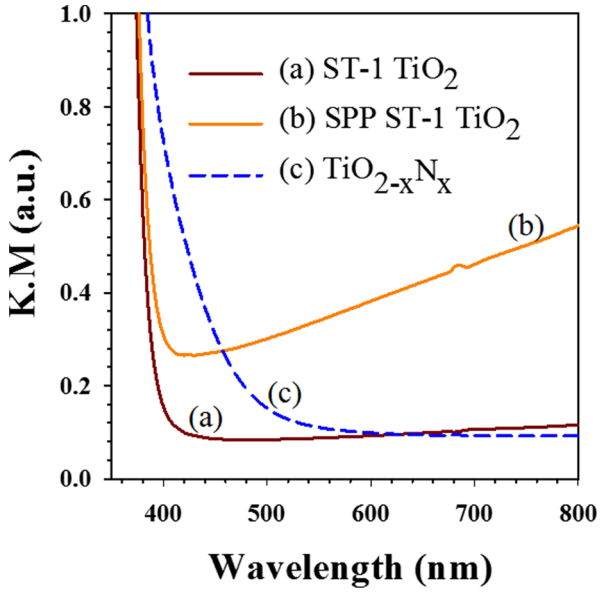

Figure 3. Optical absorbance (Kubelka−Munk) of the untreated and SPP-treated ST-1 TiO_2 feedstock powders (the dotted line represents the untreated nitrogen-doped TiO_2 powder).

the optical absorbance results (Kubelka−Munk) of the untreated and SPP-treated ST-01 TiO_2 (indicated as "a"). To understand the optical properties of the defect-induced ST-1 TiO_2 (indicated as "b"), we compared these spectra with those of nitrogen-doped TiO_2 commercial powder ($TiO_{2-x}N_x$) in Figure 3 (indicated as "c"). These results indicate that the SPP treatment markedly enhanced the optical absorbance in the visible wavelength region (400−800 nm); however, there was no noticeable shift in the characteristic band edge position, as for $TiO_{2-x}N_x$. This raises questions about the origin of the visible light absorption of the SPP-treated ST-1 TiO_2 sample. We explain this behavior based on the standard visible light-driven nitrogen-doped TiO_2 system (dotted line in Figure 3). In general, nitrogen anion doping introduces charge carriers into TiO_2 and creates mid band gap states above the valence band (i.e., band gap splitting), which are responsible for the visible light absorption of $TiO_{2-x}N_x$.[10] Compared with the absorption features of $TiO_{2-x}N_x$ in Figure 3, the SPP-treated ST-1 TiO_2 did not show any shift of the optical band edge but instead featured enhanced absorbance in the tail part of the visible light region. According to the literature, the ionization energy of oxygen vacancies in reduced TiO_2 lies between ~0.75 and 1.18 eV.[13,41,42] From this value, we can assume that oxygen vacancies are located below the conduction band as surface states. A few other researchers have reported a similar optical behavior of bicrystalline phase and oxygen vacancies introduced into TiO_2.[22,31,33,43] The creation of oxygen vacancies (V_o) by the SPP treatment was verified with electron spin resonance (ESR) measurements (Figure S6, Supporting Information). From Figure S6, additional peaks were found at $g = 2.003$ in the ESR spectra of 3 and 8 h SPP-treated ST-1 TiO_2. These results confirmed that oxygen vacancies were generated by the SPP treatment.[44] Furthermore, no major peaks were observed for Ti^{3+} at $g = 1.975$.[45] Therefore, the ESR results support the premise that the optical absorbance enhancement of ST-1 TiO_2 could be attributed to oxygen vacancy defects rather than Ti^{3+}. XPS analysis also showed that the SPP-treated ST-1 TiO_2 contained no Ti^{3+} centers.

On the other hand, the light absorbance enhancement in the tail region (400−800 nm) in ST-1 TiO_2 may also be influenced by brookite/anatase heterostructure formation. In the hetero-crystalline structure, that is, brookite/anatase (B/A) or anatase/rutile (A/R), the absorbance edge shift relies on the fraction of the composite ratio (B/A). Zhao et al.[31] reported that brookite phase quantity mainly influences the optical absorbance feature of the B/A composite. For instance, for the brookite phase, until it reaches the optimum fraction (B_{50}/A_{50}), the quantity of light absorbance is monotonically increased in the visible light region (>400 nm). While the brookite quantity exceeds the optimum ratio, the optical absorbance edge will be shifted. In the present work, the SPP treatment promotes the optical absorbance quantity in the visible light wavelength region rather than band edge shift. This implies that brookite phase formation during SPP treatment could be mild and lesser than the optimum ratio (B_{50}/A_{50}). Therefore, we conclude that the energetic structure of the SPP-treated ST-1 TiO_2 is different from that of black TiO_2.

Photocatalytic Activity. The photocatalytic activities of the untreated and SPP-treated ST-1 TiO_2 solid were evaluated for the degradation of gaseous acetaldehyde.[46] First, we investigated the influence of the SPP treatment duration time (3, 8, and 15 h) on the photocatalytic activity of ST-1 TiO_2. Figure 4 shows the typical plots of the decrease in the concentration of acetaldehyde and the increase in the concentration of CO_2 products as a function of reaction time. During the equilibrium process (in the dark), a slight decrease of the acetaldehyde concentration for the untreated ST-1 TiO_2 sample (dotted line in Figure 4) without an accompanying increase in CO_2 concentration was attributed to the gas adsorption on the TiO_2 surface. The solid line plots in Figure 4 indicate that the acetaldehyde concentration decreased as CO_2 formed when the solids were irradiated by a fluorescence lamp (8000 lux intensity). Note the 1:2 stoichiometric ratio between acetaldehyde and CO_2. From Figure 4, the untreated ST-1

DOI: 10.1021/acsomega.7b01698
ACS Omega 2018, 3, 898−905

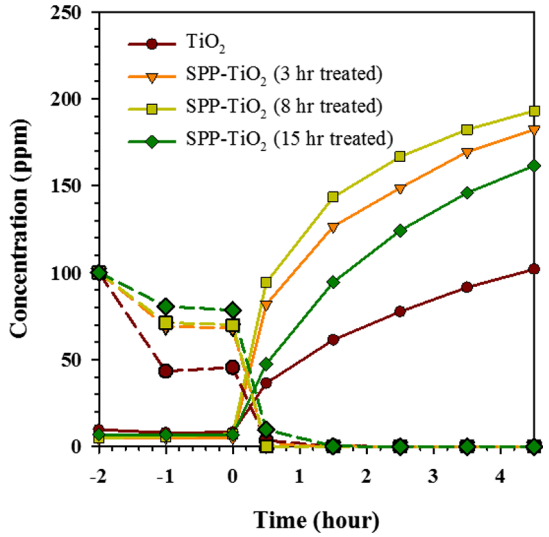

Figure 4. Plots of decreasing acetaldehyde concentration for the untreated and SPP-treated ST-1 TiO_2 samples vs time. The dashed and solid lines represent the acetaldehyde and CO_2 concentrations, respectively.

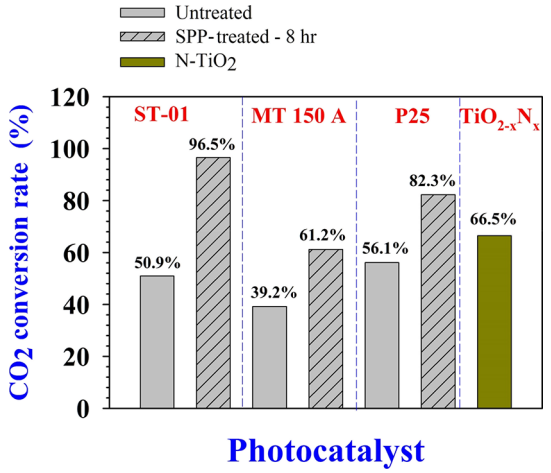

Figure 5. Quantitative comparison of CO_2 conversion rate (%) from photocatalytic acetaldehyde degradation experiments using different photocatalyst samples.

Scheme 2. Proposed Mechanism of Photocatalytic Degradation of Acetaldehyde by the SPP-Treated ST-1 TiO_2

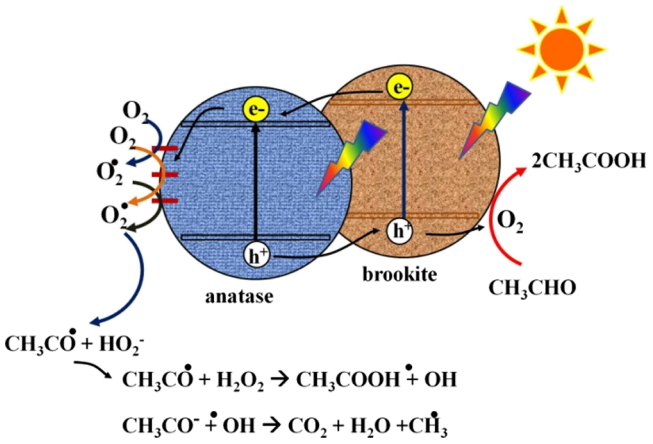

TiO_2 showed a very weak photocatalytic activity for acetaldehyde molecules and only 50.9% CO_2 conversion. Under identical experimental conditions, the 8 h SPP-treated ST-1 TiO_2 showed a high photocatalytic activity, with 96.6% of the initial acetaldehyde completely converted to CO_2. The 15 h-treated ST-1 TiO_2 sample resulted in a lower photoactivity (80.7%) than that of the 3 h (91.1%)-treated samples owing to a reduction of the surface area during the SPP treatment (Figure S7, Supporting Information). The difference of the photocatalytic performance between 3 and 8 h samples is found to be ~5%. This implies that 3 h of SPP treatment is sufficient to achieve effective photocatalytic degradation compared to the untreated sample.

We investigated the feasibility of using this SPP technique to treat other commercial TiO_2 feedstock powders. We examined the properties of TiO_2 after the SPP treatment, for P25-TiO_2 and MT-150A TiO_2. P25 TiO_2 featured a mixture of anatase and rutile phases, and MT-150A-TiO_2 consists of a pure rutile phase. The photocatalytic results of the untreated and SPP-treated samples for the degradation of acetaldehyde to CO_2 are presented in Figure 5. This bar chart indicates that the SPP treatment markedly enhanced the photocatalytic performance of all samples. However, the 3 h SPP-treated ST-1 TiO_2 showed the highest photocatalytic performance among all SPP-treated TiO_2 feedstock samples. On the basis of these results, the photocatalytic performance of the TiO_2 could be ordered as ST-1 > P25 > N-TiO_{2-x} > MT-150A. The SPP-treated P25 and MT-150A TiO_2 both showed a high visible light activity (Figure S8, Supporting Information); however, their photocatalytic activities were lower than that of ST-1 TiO_2. Similarly, the untreated nitrogen-doped TiO_2 (N-TiO_2) also possessed a high visible light activity at 420 nm but had low photocatalytic performance.

A possible mechanism for the photocatalytic degradation of the gaseous acetaldehyde by the SPP-treated ST-1 TiO_2 is shown in Scheme 2 and can be explained as follows. Under light irradiation, photogenerated electrons (e^-) and holes (h^+) are, respectively, induced in the conduction and valence bands of ST-1 TiO_2. These charge carriers drive the photocatalytic degradation of the gaseous acetaldehyde reaction in a multistep transformation. Various potential pathways for photocatalytic degradation by TiO_2 have been proposed, including hole-generated hydroxyl radicals, carbonyl radicals, superoxide radicals, and hydrogen peroxide.[47,48] A typical reaction scheme is described as follows:[49] (i) photogenerated holes mediate the reaction:

$$3CH_3CO + O_2 + h^+ \rightarrow 2CH_3COOH + CH_3CO^\bullet + H^+ \quad (1)$$

and (ii) photoelectrons mediate the reaction:

$$e^- + O_2 \rightarrow O_2^\bullet \quad (2)$$

$$2CH_3CHO + O_2 \rightarrow 2CH_3COOH \quad (3)$$

The carbonyl radicals ($CH_3CO^\bullet$) formed in eq 1 can react with O_2, which mediates the chain reactions of acetaldehyde oxidation. In these multiple reactions, acetic acid is the main intermediate in the transformation to CO_2, by the reaction $CH_3COOH + \bullet OH \rightarrow CO_2 + H_2O + CH_3^\bullet$.

We confirmed that the SPP treatment produced oxygen vacancies and surface defects below the conduction band. These defects led to the formation of more reactive sites and attracted atmospheric oxygen species, which were converted to

DOI: 10.1021/acsomega.7b01698
ACS Omega 2018, 3, 898−905

O_2^* radicals through reactions with photoelectrons (eq 2). These oxygen radicals are a key intermediate driving the acetaldehyde degradation reactions in the SPP-treated TiO_2 samples. Therefore, we conclude that the high gaseous photocatalytic performance shown by the SPP-treated ST-1 TiO_2 can be attributed to the following reasons: (a) a greater number of reactive sites through the formation of surface defects (b) more effective charge separation at anatase/brookite heterocrystalline phases; and (c) enhanced hydrophilicity of the surface (Ti−OH formation). To determine the effects of the light wavelength on the 3 h SPP-treated ST-1 TiO_2, we examined the photocatalytic activity at different light irradiation wavelengths (Figure S9, Supporting Information). We found that the photocatalytic activity was highest in the UV region (<420 nm) and no activity occurred in the visible region (>420 nm). Although the sample showed considerable absorption of visible light, attributed to oxygen vacancy surface states, the photocatalytic activity was driven by excitation in the UV light region. These results suggest that the crystalline phases (anatase/brookite) and lattice arrangement (defects) induced by the SPP treatment were responsible for the enhanced activity rather than the increased visible light absorption. Though significant visible light absorbance was observed in SPP-treated TiO_2 (Figures 3 and S8), it does not show a gas-phase photocatalytic activity at 400 nm. This discrepancy may be due to the fact that the quantity of light absorbance in the visible light wavelength region (400−800 nm) is still not sufficient compared to black TiO_2 to drive the gas-phase photocatalysis reaction using only visible light photons.[50]

CONCLUSIONS

We used a room-temperature SPP technique to produce a heterocrystalline anatase/brookite TiO_2 solid, containing oxygen vacancies, on a large scale. This process has advantages in terms of its room-temperature processing, potential for scale-up, and relatively short processing time compared with conventional vacuum-based high-temperature approaches. Thus, we show that the SPP is an effective modern tool for material modification, which avoids the risks of handling gas-phase hydrogen species in high-temperature plasma treatments. However, further investigations are required to examine the underlying mechanism of the TiO_2 lattice rearrangement induced by the SPP treatment from both theoretical and experimental approaches (e.g., X-ray absorption techniques). Further studies of the SPP parameters, such as different feedstocks, cathode materials, and interdependence of SPP treatment duration and crystalline phase ratio, will be conducted in the future to optimize the photocatalytic performance. The SPP technique enables a wide range of feedstock powders to be used as starting materials. Hence, the SPP technique is shown to be a simple tool with the potential for low-cost modification of a wide range of metal oxides and possibly other materials such as narrow-band gap metal sulfides, carbonaceous materials, and polymer materials.

EXPERIMENTAL SECTION

Solution Plasma Processing. We adopt the SPP technique reported elsewhere[51] and demonstrate with a major modification. Primarily, the plasma was generated in deionized water using a pulsed dc power supply (Kurita Co. Ltd; MPP-HV04). Tungsten (W) tubes (outer diameter: 3 mm and inner diameter: 1 mm) were used as electrodes with an interelectrode gap of 0.3 mm. To expose the plasma only on the tip of the tungsten electrode, the remaining part of the electrode was covered with a ceramic insulator tube. Nitrogen gas (flow rate: 200 mL min^{-1}) was applied through the cavity (0.1 mm) of the tungsten cathode. The applied voltage, pulse frequency, and pulse width were optimized for effective plasma generation and are as follows: V = 2 kV, F = 20 kHz, and t = 1 μs, respectively. The plasma was generated for different time durations (3, 8, and 15 h) based on the requirement. The schematic illustration of the SPP apparatus setup is given in Scheme 1. The feedstock TiO_2 powder was continuously circulated through a motor.

Characterization. The crystal structures of the untreated and SPP-treated samples were examined using an X-ray diffractometer (Rigaku Ultima IV). The crystalline morphology and lattice were analyzed using a HAADF−scanning transmission electron microscope (HF-2210, Hitachi, Ltd. Japan). The chemical environment of pristine and SPP-treated samples was analyzed using XPS with a monochromated Al Kα source (AXIS Nova, Kratos Analytical). The optical absorbance of the samples were recorded using the diffuse reflectance spectra of the electrodes in the range of 350−800 nm using a V-670 JASCO UV−vis spectrophotometer. The absorbance of the untreated and SPP-treated TiO_2 samples was obtained through the Kubelka−Munk relationship with in-built software from the JASCO UV−vis spectrometer. The ESR spectra of the untreated and SPP-treated sample were recorded with an ESP350E (Bruker Co.) at 20 K under the following conditions: central magnetic field, 3386 G; magnetic field sweep width, 200 G; and microwave frequency and power: 9.48 GHz and 4 μW, respectively. The surface areas of the untreated and SPP-treated samples were evaluated by the Brunauer−Emmett−Teller technique using a BELSORP-max instrument.

Photocatalytic Experiments. The photocatalytic activity was evaluated by degradation of gaseous acetaldehyde in a batch-type reactor. The Pyrex glass-based vessel (500 mL volume) was used for the experiment, and its top was covered with a quartz plate. An equal amount of TiO_2 samples was used for all photocatalytic experiments. For instance, 0.1 g of TiO_2 powder sample mixed with 0.2 mL of deionized water was spread on the glass substrate and dried at 60 °C. Further, this sample was kept at the bottom of the glass vessel as explained above. Before starting the degradation experiments, the vessel was filled with commercially available pure air (Taiyo Nippon Sanso Corp.) with a humidity of about 50% by flowing through a water mixture. Followed that, the samples were illuminated in air using UV light (1.2 mW cm^2) for 24 h to remove the unwanted organic pollutants on the surface. Then, a measured amount of gaseous acetaldehyde (1 vol % acetaldehyde in N_2, Takachiho) was injected into the reactor with a Pressure-Lok syringe as the target pollutant. The system was kept in the dark for 1 h for adsorption equilibration and then was irradiated with a fluorescent lamp (8000 lux). The decrease in the acetaldehyde concentration and the increase in the CO_2 product concentration were monitored using gas chromatography with nitrogen as a carrier (GC-2014, Shimadzu, equipped with a 2 m Porapak-Q column and a flame ionization detector). Three batches of the untreated and SPP-treated TiO_2 samples were tested, and the average values are presented.

ASSOCIATED CONTENT

Supporting Information

The Supporting Information is available free of charge on the ACS Publications website at DOI: 10.1021/acsomega.7b01698.

DOI: 10.1021/acsomega.7b01698
ACS Omega 2018, 3, 898−905

Photograph of the samples, XRD results, HAADF−STEM images, ESR results, surface area results, optical absorbance spectra, and light irradiation wavelength-dependent photocatalytic activity (PDF)

Plasma generation from the SPP reaction chamber captured by a high-speed camera (AVI)

AUTHOR INFORMATION

Corresponding Author

*E-mail: terashima@rs.tus.ac.jp (C.T.).

ORCID

Kazuya Nakata: 0000-0002-6648-8534

Nagahiro Saito: 0000-0001-8757-3933

Chiaki Terashima: 0000-0002-8874-1481

Present Address

#Multifunctional Photocatalyst and Coatings Group, SPECIFIC, College of Engineering, Swansea University (Bay Campus), Swansea SA1 8EN, Wales, United Kingdom (S.P.).

Notes

The authors declare no competing financial interest.

ACKNOWLEDGMENTS

This work was supported by the Strategic International Collaborative Research Program (SICORP) by JST. C.T. acknowledges the partial financial support from JSPS KAKENHI 26410247. The authors thank Dr. T. Ichihashi for the TEM analysis and Y. Sakurai for the XPS measurements.

REFERENCES

(1) Fujishima, A.; Honda, K. Electrochemical Photolysis of Water at a Semiconductor Electrode. *Nature* **1972**, *238*, 37−38.

(2) Kudo, A.; Miseki, Y. Heterogeneous photocatalyst materials for water splitting. *Chem. Soc. Rev.* **2009**, *38*, 253−278.

(3) Fujihira, M.; Satoh, Y.; Osa, T. Heterogeneous photocatalytic oxidation of aromatic compounds on TiO2. *Nature* **1981**, *293*, 206−208.

(4) Chen, X.; Li, Y.; Pan, X.; Cortie, D.; Huang, X.; Yi, Z. Photocatalytic oxidation of methane over silver decorated zinc oxide nanocatalysts. *Nat. Commun.* **2016**, *7*, 12273.

(5) Tatsuma, T.; Saitoh, S.; Ngaotrakanwiwat, P.; Ohko, Y.; Fujishima, A. Energy Storage of TiO2−WO3 Photocatalysis Systems in the Gas Phase. *Langmuir* **2002**, *18*, 7777−7779.

(6) Wang, R.; Hashimoto, K.; Fujishima, A.; Chikuni, M.; Kojima, E.; Kitamura, A.; Shimohigoshi, M.; Watanabe, T. Light-induced amphiphilic surfaces. *Nature* **1997**, *388*, 431−432.

(7) Devadoss, A.; Sudhagar, P.; Terashima, C.; Nakata, K.; Fujishima, A. Photoelectrochemical biosensors: New insights into promising photoelectrodes and signal amplification strategies. *J. Photochem. Photobiol., C* **2015**, *24*, 43−63.

(8) Jukapli, N. M.; Bagheri, S. Recent developments on titania nanoparticle as photocatalytic cancer cells treatment. *J. Photochem. Photobiol., B* **2016**, *163*, 421−430.

(9) Miyauchi, M.; Irie, H.; Liu, M.; Qiu, X.; Yu, H.; Sunada, K.; Hashimoto, K. Visible-Light-Sensitive Photocatalysts: Nanocluster-Grafted Titanium Dioxide for Indoor Environmental Remediation. *J. Phys. Chem. Lett.* **2016**, *7*, 75−84.

(10) Asahi, R.; Morikawa, T.; Ohwaki, T.; Aoki, K.; Taga, Y. Visible-Light Photocatalysis in Nitrogen-Doped Titanium Oxides. *Science* **2001**, *293*, 269.

(11) Khan, S. U. M.; Al-Shahry, M.; Ingler, W. B. Efficient Photochemical Water Splitting by a Chemically Modified n-TiO_2. *Science* **2002**, *297*, 2243.

(12) Sathasivam, S.; Bhachu, D. S.; Lu, Y.; Chadwick, N.; Althabaiti, S. A.; Alyoubi, A. O.; Basahel, S. N.; Carmalt, C. J.; Parkin, I. P. Tungsten Doped TiO2 with Enhanced Photocatalytic and Optoelectrical Properties via Aerosol Assisted Chemical Vapor Deposition. *Sci. Rep.* **2015**, *5*, 10952.

(13) Pan, X.; Yang, M.-Q.; Fu, X.; Zhang, N.; Xu, Y.-J. Defective TiO2 with oxygen vacancies: synthesis, properties and photocatalytic applications. *Nanoscale* **2013**, *5*, 3601−3614.

(14) Pan, X.; Yang, M.-Q.; Xu, Y.-J. Morphology control, defect engineering and photoactivity tuning of ZnO crystals by graphene oxide—a unique 2D macromolecular surfactant. *Phys. Chem. Chem. Phys.* **2014**, *16*, 5589−5599.

(15) Yuan, L.; Han, C.; Yang, M.-Q.; Xu, Y.-J. Photocatalytic water splitting for solar hydrogen generation: fundamentals and recent advancements. *Int. Rev. Phys. Chem.* **2016**, *35*, 1−36.

(16) Liu, S.; Han, C.; Tang, Z.-R.; Xu, Y.-J. Heterostructured semiconductor nanowire arrays for artificial photosynthesis. *Mater. Horiz.* **2016**, *3*, 270−282.

(17) Tao, J.; Luttrell, T.; Batzill, M. A two-dimensional phase of TiO2 with a reduced bandgap. *Nat. Chem.* **2011**, *3*, 296−300.

(18) Chen, X.; Liu, L.; Yu, P. Y.; Mao, S. S. Increasing Solar Absorption for Photocatalysis with Black Hydrogenated Titanium Dioxide Nanocrystals. *Science* **2011**, *331*, 746.

(19) Liu, N.; Schneider, C.; Freitag, D.; Venkatesan, U.; Marthala, V. R. R.; Hartmann, M.; Winter, B.; Spiecker, E.; Osvet, A.; Zolnhofer, E. M.; Meyer, K.; Nakajima, T.; Zhou, X.; Schmuki, P. Hydrogenated Anatase: Strong Photocatalytic Dihydrogen Evolution without the Use of a Co-Catalyst. *Angew. Chem.* **2014**, *126*, 14425−14429.

(20) Chen, X.; Liu, L.; Liu, Z.; Marcus, M. A.; Wang, W.-C.; Oyler, N. A.; Grass, M. E.; Mao, B.; Glans, P.-A.; Yu, P. Y.; Guo, J.; Mao, S. S. Properties of Disorder-Engineered Black Titanium Dioxide Nanoparticles through Hydrogenation. *Sci. Rep.* **2013**, *3*, 1510.

(21) Liu, N.; Häublein, V.; Zhou, X.; Venkatesan, U.; Hartmann, M.; Mačković, M.; Nakajima, T.; Spiecker, E.; Osvet, A.; Frey, L.; Schmuki, P. "Black" TiO2 Nanotubes Formed by High-Energy Proton Implantation Show Noble-Metal-co-Catalyst Free Photocatalytic H2-Evolution. *Nano Lett.* **2015**, *15*, 6815−6820.

(22) Dong, J.; Han, J.; Liu, Y.; Nakajima, A.; Matsushita, S.; Wei, S.; Gao, W. Defective Black TiO2 Synthesized via Anodization for Visible-Light Photocatalysis. *ACS Appl. Mater. Interfaces* **2014**, *6*, 1385−1388.

(23) Takai, O. Solution plasma processing (SPP). *Pure Appl. Chem.* **2008**, *80*, 2003.

(24) Chen, Q.; Li, J.; Li, Y. A review of plasma−liquid interactions for nanomaterial synthesis. *J. Phys. D: Appl. Phys.* **2015**, *48*, 424005.

(25) Morishita, T.; Ueno, T.; Panomsuwan, G.; Hieda, J.; Yoshida, A.; Bratescu, M. A.; Saito, N. Fastest Formation Routes of Nanocarbons in Solution Plasma Processes. *Sci. Rep.* **2016**, *6*, 36880.

(26) Saito, G.; Nakasugi, Y.; Yamashita, T.; Akiyama, T. Solution plasma synthesis of bimetallic nanoparticles. *Nanotechnology* **2014**, *25*, 135603.

(27) Sudare, T.; Ueno, T.; Watthanaphanit, A.; Saito, N. Accelerated nanoparticles synthesis in alcohol−water-mixture-based solution plasma. *Phys. Chem. Chem. Phys.* **2015**, *17*, 30255−30259.

(28) Panomsuwan, G.; Watthanaphanit, A.; Ishizaki, T.; Saito, N. Water-plasma-assisted synthesis of black titania spheres with efficient visible-light photocatalytic activity. *Phys. Chem. Chem. Phys.* **2015**, *17*, 13794−13799.

(29) Ishida, Y.; Doshin, W.; Tsukamoto, H.; Yonezawa, T. Black TiO2 Nanoparticles by a Microwave-induced Plasma over Titanium Complex Aqueous Solution. *Chem. Lett.* **2015**, *44*, 1327−1329.

(30) Zhou, P.; Xie, Y.; Liu, L.; Song, J.; Chen, T.; Ling, Y. Bicrystalline TiO2 heterojunction for enhanced organic photodegradation: engineering and exploring surface chemistry. *RSC Adv.* **2017**, *7*, 16484−16493.

(31) Zhao, H.; Liu, L.; Andino, J. M.; Li, Y. Bicrystalline TiO2 with controllable anatase−brookite phase content for enhanced CO2 photoreduction to fuels. *J. Mater. Chem. A* **2013**, *1*, 8209−8216.

(32) Li, Z.; Cong, S.; Xu, Y. Brookite vs Anatase TiO2 in the Photocatalytic Activity for Organic Degradation in Water. *ACS Catal.* **2014**, *4*, 3273−3280.

(33) Zhou, W.; Gai, L.; Hu, P.; Cui, J.; Liu, X.; Wang, D.; Li, G.; Jiang, H.; Liu, D.; Liu, H.; Wang, J. Phase transformation of TiO2

DOI: 10.1021/acsomega.7b01698
ACS Omega 2018, 3, 898−905

nanobelts and TiO2(B)/anatase interface heterostructure nanobelts with enhanced photocatalytic activity. *CrystEngComm* **2011**, *13*, 6643−6649.
(34) Saito, N.; Hieda, J.; Takai, O. Synthesis process of gold nanoparticles in solution plasma. *Thin Solid Films* **2009**, *518*, 912−917.
(35) Bratescu, M. A.; Cho, S.-P.; Takai, O.; Saito, N. Size-Controlled Gold Nanoparticles Synthesized in Solution Plasma. *J. Phys. Chem. C* **2011**, *115*, 24569−24576.
(36) Saito, G.; Nakasugi, Y.; Akiyama, T. Generation of solution plasma over a large electrode surface area. *J. Appl. Phys.* **2015**, *118*, 023303.
(37) Hu, W.; Liu, Y.; Withers, R. L.; Frankcombe, T. J.; Norén, L.; Snashall, A.; Kitchin, M.; Smith, P.; Gong, B.; Chen, H.; Schiemer, J.; Brink, F.; Wong-Leung, J. Electron-pinned defect-dipoles for high-performance colossal permittivity materials. *Nat. Mater.* **2013**, *12*, 821−826.
(38) Yu, J.; Yu, J. C.; Ho, W.; Jiang, Z. Effects of calcination temperature on the photocatalytic activity and photo-induced super-hydrophilicity of mesoporous TiO2 thin films. *New J. Chem.* **2002**, *26*, 607−613.
(39) Luciu, I.; Bartali, R.; Laidani, N. Influence of hydrogen addition to an Ar plasma on the structural properties of TiO_{2-x} thin films deposited by RF sputtering. *J. Phys. D: Appl. Phys.* **2012**, *45*, 345302.
(40) Fujishima, A.; Zhang, X.; Tryk, D. TiO2 photocatalysis and related surface phenomena. *Surf. Sci. Rep.* **2008**, *63*, 515−582.
(41) Deng, Z. H.; Li, L.; Ding, W.; Xiong, K.; Wei, Z. D. Synthesized ultrathin MoS2 nanosheets perpendicular to graphene for catalysis of hydrogen evolution reaction. *Chem. Commun.* **2015**, *51*, 1893−1896.
(42) Takeuchi, K.; Nakamura, I.; Matsumoto, O.; Sugihara, S.; Ando, M.; Ihara, T. Preparation of Visible-Light-Responsive Titanium Oxide Photocatalysts by Plasma Treatment. *Chem. Lett.* **2000**, 1354−1355.
(43) Yang, X.; Salzmann, C.; Shi, H.; Wang, H.; Green, M. L. H.; Xiao, T. The Role of Photoinduced Defects in TiO2 and Its Effects on Hydrogen Evolution from Aqueous Methanol solution. *J. Phys. Chem. A* **2008**, *112*, 10784−10789.
(44) Hurum, D. C.; Agrios, A. G.; Gray, K. A.; Rajh, T.; Thurnauer, M. C. Explaining the Enhanced Photocatalytic Activity of Degussa P25 Mixed-Phase TiO2 Using EPR. *J. Phys. Chem. B* **2003**, *107*, 4545−4549.
(45) Khan, M. M.; Ansari, S. A.; Pradhan, D.; Ansari, M. O.; Han, D. H.; Lee, J.; Cho, M. H. Band gap engineered TiO2 nanoparticles for visible light induced photoelectrochemical and photocatalytic studies. *J. Mater. Chem. A* **2014**, *2*, 637−644.
(46) Liu, Z.; Zhang, X.; Nishimoto, S.; Murakami, T.; Fujishima, A. Efficient Photocatalytic Degradation of Gaseous Acetaldehyde by Highly Ordered TiO2 Nanotube Arrays. *Environ. Sci. Technol.* **2008**, *42*, 8547−8551.
(47) Sopyan, I.; Watanabe, M.; Murasawa, S.; Hashimoto, K.; Fujishima, A. An efficient TiO2 thin-film photocatalyst: photocatalytic properties in gas-phase acetaldehyde degradation. *J. Photochem. Photobiol., A* **1996**, *98*, 79−86.
(48) Ohko, Y.; Tryk, D. A.; Hashimoto, K.; Fujishima, A. Autoxidation of Acetaldehyde Initiated by TiO2 Photocatalysis under Weak UV Illumination. *J. Phys. Chem. B* **1998**, *102*, 2699−2704.
(49) Zhao, T.; Liu, Z.; Nakata, K.; Nishimoto, S.; Murakami, T.; Zhao, Y.; Jiang, L.; Fujishima, A. Multichannel TiO2 hollow fibers with enhanced photocatalytic activity. *J. Mater. Chem.* **2010**, *20*, 5095−5099.
(50) Wang, Z.; Yang, C.; Lin, T.; Yin, H.; Chen, P.; Wan, D.; Xu, F.; Huang, F.; Lin, J.; Xie, X.; Jiang, M. H-Doped Black Titania with Very High Solar Absorption and Excellent Photocatalysis Enhanced by Localized Surface Plasmon Resonance. *Adv. Funct. Mater.* **2013**, *23*, 5444−5450.
(51) Cho, S.-P.; Bratescu, M. A.; Saito, N.; Takai, O. Microstructural characterization of gold nanoparticles synthesized by solution plasma processing. *Nanotechnology* **2011**, *22*, 455701.

DOI: 10.1021/acsomega.7b01698
ACS Omega 2018, 3, 898−905